heritage

MDPI

Article

Assessing Carbonation Maturity for Restoration Compatibility: A Spectroscopic–Mineralogical Study of Historic and Modern Lime Mortars

İrem Ceran [1,2,*] and Ersin Kaygisiz [1]

[1] Research Center for the Conservation of Cultural Property of Foundation, Fatih Sultan Mehmet Vakıf University, Istanbul 34015, Türkiye; ekaygisiz@fsm.edu.tr
[2] Faculty of Arts, Design and Architecture—Restoration and Conservation of Cultural Assets, Fatih Sultan Mehmet Vakıf University, Istanbul 34015, Türkiye
* Correspondence: iceran@fsm.edu.tr

Abstract

Understanding the carbonation behavior of lime-based mortars is essential for ensuring material compatibility and long-term durability in architectural restoration. This study presents a comparative spectroscopic and mineralogical analysis of eleven mortar samples collected from both the original (11th–12th century) and modern extension walls of a historic structure. X-ray diffraction (XRD) and attenuated total reflectance–Fourier transform infrared spectroscopy (ATR-FTIR) were employed to assess the mineralogical composition and carbonation maturity. The results indicate that the historic mortars have undergone complete carbonation, as evidenced by sharp and well-defined calcite bands, whereas the modern repair mortars display broader carbonate peaks, suggesting ongoing carbonation processes. XRD analysis confirmed the dominance of calcite and gypsum, along with the presence of illite, albite, and microcline, indicating mineralogical signatures of both binder transformations (such as carbonation and sulfate formation) and aggregate contributions. The weak water absorption bands and limited sulfate signals observed in the spectra further suggest advanced aging and mineral stabilization in the historic mortars. These findings highlight the differing carbonation kinetics between historic and modern lime mortars and emphasize the importance of selecting repair materials with compatible chemical and physical aging characteristics. The combined use of XRD and ATR-FTIR proves to be an effective diagnostic approach to guide restoration material selection and support the long-term integrity of masonry structures.

Keywords: lime mortar; carbonation; material compatibility; historic masonry; ATR-FTIR; XRD

Academic Editor: João Pedro Veiga

Received: 28 May 2025
Revised: 8 July 2025
Accepted: 14 July 2025
Published: 27 February 2026

1. Introduction

The analysis of historic lime-based mortars plays a crucial role in understanding the physicochemical transformations that occur over time due to environmental factors and material aging. One of the most significant of these transformations is the carbonation process, in which atmospheric CO_2 reacts with calcium hydroxide ($Ca(OH)_2$) to form calcium carbonate ($CaCO_3$) [1]. Carbonation directly affects the mechanical properties, durability, and conservation strategies of historic structures. Therefore, a detailed examination of this process in historic mortars is essential for assessing material performance and understanding deterioration mechanisms.

Lime has played a significant role in the construction industry throughout history, often combined with various materials such as clay, pozzolan, charcoal, gravel, and straw. Depending on its application (structural elements, plaster, or ground filling), it has been mixed with different components to enhance its properties. Today, lime is primarily used in the restoration of historic buildings and monuments. However, the growing demand for sustainable construction materials, coupled with lime's ability to absorb CO_2 through the carbonation process, has brought lime-based binders back into focus as a potential solution in the fight against climate change [2]. Lime, a calcium-based inorganic material, has been widely used since ancient times. As early as 7500 BCE, a plaster made from lime and unheated crushed limestone was discovered in what is now modern-day Jordan [3]. During the period of Ancient Greece (2800–1000 BCE), the use of lime gradually spread on a small scale. It was recognized that lime mortar not only provided durability but also enhanced the overall aesthetic appearance of buildings [4]. The Romans effectively utilized the advantages of lime and mastered construction techniques. In their building processes, they combined lime with sand and pozzolanic materials to develop a durable type of concrete known as Roman mortar. During the Middle Ages (approximately 1300–1800 CE), lime played a crucial role as a building material in the construction of houses [5,6].

Over time, various analytical techniques have been applied for the analysis of historic mortars. These include methods such as X-ray diffraction (XRD) and Fourier transform infrared spectroscopy (FTIR) [7–9]. The XRD method is widely used to identify major mineral phases in lime-based mortars, such as portlandite ($Ca(OH)_2$), calcite ($CaCO_3$), and gypsum ($CaSO_4 \cdot 2H_2O$). On the other hand, FTIR spectroscopy, particularly when combined with attenuated total reflection (ATR) technology, is becoming increasingly important in mortar characterization due to its ability to non-destructively analyze the fundamental vibrational modes of carbonates, sulfates, and silicates [10]. The mid-infrared region (4000–400 cm^{-1}) is widely used in spectroscopic analysis due to the distinct specificity of spectral bands. ATR-FTIR spectroscopy offers a significant advantage in the analysis of heterogeneous materials such as historic mortars, as it allows for direct sample measurement without requiring an extensive preparation process [11,12]. The carbonation process exhibits distinct characteristics in the FTIR spectrum at specific wavelengths. Notably, the asymmetric stretching vibration of the CO_3^{2-} ion appears in the 1400–1500 cm^{-1} range, the in-plane bending vibration is observed at 875 cm^{-1}, and the out-of-plane bending vibration is detected at 713 cm^{-1} [7,13]. However, in silica-rich matrices, the overlap of spectral bands from various mineral components can complicate the interpretation of ATR-FTIR analyses [14]. In addition to carbonation, the presence of gypsum ($CaSO_4 \cdot 2H_2O$) plays a crucial role in the deterioration of mortars. Gypsum can form either as a result of the reaction between lime-based mortars and sulfur-containing pollutants or due to the original composition of the mortar [15,16]. Gypsum detection using ATR-FTIR is typically based on sulfate (SO_4^{2-}) absorption bands in the 1100–1150 cm^{-1} range and the bending mode in the 600–670 cm^{-1} region. The presence of gypsum alongside calcite may indicate secondary alteration processes in the mortar, such as sulfation, which can lead to the gradual weakening of the mortar structure over time [9].

There is a limited number of studies in the literature that directly compare the carbonation processes of historical and modern mortars using a combined approach of XRD and ATR-FTIR spectroscopy. Existing research typically employs these techniques separately or focuses exclusively on the characterization of historical mortars. For instance, in one study, historical mortars from the Castellón region of Spain were characterized using FTIR analysis supported by XRD, yet no direct comparison with modern intervention mortars was made [17]. Similarly, ancient mortar samples from the Church of the Cross in Gerasa, Jordan, were analyzed using FTIR and thermogravimetric analysis (TGA), but without any comparative evaluation against

modern mortars [18]. Therefore, the scarcity of studies that integrate XRD and ATR-FTIR to directly assess the carbonation maturity of both historical and modern mortars highlights the significance and potential contribution of new research in this area.

This study presents a novel analytical approach that combines X-ray diffraction (XRD) and attenuated total reflectance–Fourier transform infrared spectroscopy (ATR-FTIR) to evaluate the carbonation process in historic lime-based mortars. By integrating mineralogical and molecular-level data, this dual-technique framework enables a more comprehensive assessment of carbonation maturity and material aging. Adopting a case study methodology, mortar samples collected from both original sections (11th–12th century) and a later addition (mid-20th century) of a historic structure were comparatively analyzed to determine the degree of carbonation and identify secondary phases such as gypsum. In the absence of complementary elemental analysis, mineral phases identified through XRD were correlated with the corresponding ATR-FTIR spectra. The results revealed a notably lower degree of carbonation in modern intervention mortars compared to the original historical ones, highlighting differences in material behavior over time. These findings provide critical insights into the long-term durability and degradation mechanisms of lime-based mortars and offer a scientifically grounded basis for evaluating the chemical and structural compatibility of contemporary repair mortars in heritage conservation practices. This study addresses this gap by introducing a combined spectroscopic methodology that not only enhances diagnostic resolution but also bridges a critical disconnect in the literature. The novelty of this research lies in its dual-scale approach—linking molecular vibrational patterns with crystalline phase identification—to evaluate long-term material compatibility in real restoration contexts. In doing so, it offers a replicable and scientifically grounded framework for future studies aiming to improve the sustainability and performance of conservation materials.

Historical and Architectural Background

Kilise Camii, also known as Vefa Kilise Camii, is located in the Vefa neighborhood of the Süleymaniye district in Fatih, Istanbul (Figure 1). The original Byzantine-era name of Kilise Camii remains uncertain, but based on the urban planning of that period, it was situated in the X. Regio [19,20]. It is also known today as Molla Şemsettin Gürani Camii [20]. It is a former Eastern Orthodox church that was converted into a mosque during the Ottoman period. Although the exact date of its construction remains unknown, architectural features suggest that it was built in the 11th or 12th century, during the reign of Alexios I Komnenos [21]. The three-aisled naos and narthex, which form the main part of the structure, are believed to have been built in the 11th century. The additions on the north and south sides have been suggested to be later repairs made following the Latin occupation.

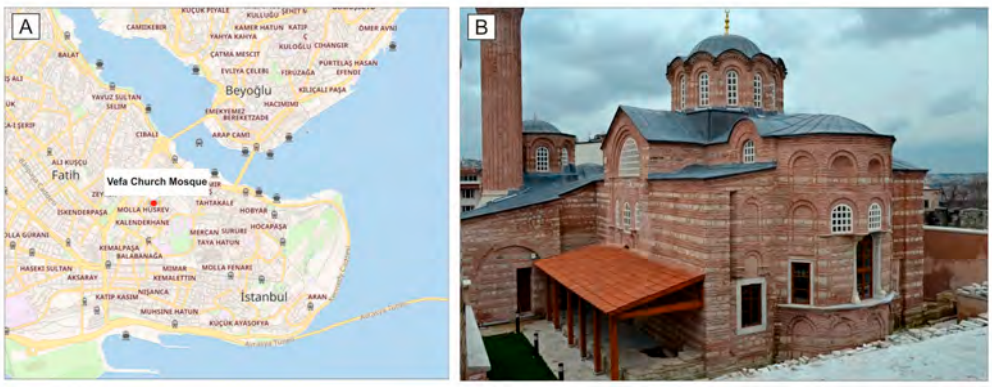

Figure 1. (**A**) Location map of Vefa Church Mosque [22]. (**B**) Vefa Church Mosque's current appearance after restoration [23].

The outermost narthex, constructed around 1320, represents the final Byzantine-era addition to the building [20]. The building was converted into a mosque in 1484, following the Ottoman conquest of Istanbul, by Şeyhülislam Molla Şemseddin Gürani, the tutor of Sultan Mehmed the Conqueror. As part of this conversion, the minaret, which still stands today, was added to the structure. According to Hadikatü'l Cevami, the mosque's minbar was installed by Abdurrahman Efendi, the son of Mehmed Eminzade Hüseyin Ağa [24].

The building, for which little information is available regarding later periods, was recorded as having been severely damaged in the 1833 fire [20]. The building was restored to approximately its present form in the second half of the 19th century and continued to undergo various repairs until the early 20th century. In 1937, Nomidis, who conducted studies on the structure, uncovered burial chambers in the basement and mosaics on the domes of the outer narthex by removing the layers of whitewash covering them. The building was also recorded as having been officially registered in the same year [25]. The most recent restoration of the building, carried out in 1972–73, appears to have been conducted without a formal project and in a superficial manner, primarily focusing on joint repairs on the exterior facades [20].

2. Materials and Methods

To investigate the carbonation process in historic laying mortar samples, X-ray diffraction (XRD) and attenuated total reflectance-Fourier transform infrared spectroscopy (ATR-FTIR) analyses were conducted as complementary techniques. These methods were chosen due to their efficiency in identifying both crystalline phases and functional groups, allowing for a comprehensive characterization of mortar composition and carbonation levels. This study specifically focuses on the laying mortars collected before the restoration activities carried out on the structure in 2015 (Figures 2 and 3). A total of eleven mortar samples were collected from different orientations of the structure: five from the north side, two from the west, one from the east, and three from the South (Table 1). All samples were extracted from approximately 5 cm beneath the surface to avoid surface contamination and weathering effects. Before the restoration, the relevant architecture firm applied to the Research Center for the Conservation of Cultural Property at Fatih Sultan Mehmet Vakıf University to request a material analysis report. The report was prepared by the institution, and a copy was archived [26].

The samples were analyzed and documented at the Research Center for the Conservation of Cultural Property at Fatih Sultan Mehmet Vakıf University. Before analysis, the samples were finely ground and stored in sealed, specialized bags to prevent contamination and environmental exposure. The primary objective was to determine the mineralogical composition of the bedding mortars from the 11th–12th century structure using XRD analysis.

ATR-FTIR spectroscopy was further employed to identify functional groups associated with calcite ($CaCO_3$) and gypsum ($CaSO_4 \cdot 2H_2O$). Calcite is the main product formed during the carbonation process of lime-based binders, while gypsum does not directly participate in carbonation but can influence setting behavior and microstructural characteristics, especially in the presence of alumina compounds or pozzolanic additives.

Additionally, two-layer mortar samples were collected from a wall added to the northern section of the structure during the second half of the 20th century. The carbonation levels of these samples were compared with those of the original historic mortars to evaluate potential compositional and chemical differences. The samples were analyzed as bulk powders, including both binder and aggregates. Through these analyses, the study aimed to provide a detailed assessment of the mineralogical and chemical composition of the

laying mortars, verify their consistency with XRD findings, and characterize the effects of carbonation prior to restoration efforts.

Figure 2. Architectural plan of Vefa Kilise Mosque and the chronological representation of its structural elements (modified from [20]). The analyzed laying mortars are marked with red dots, and sample numbers are indicated.

Table 1. The studied samples, their locations within the structure, sampling dates, and original functions.

Sample ID	Location	Sampling Date	Original Use or Function
MG-1	the outer face of the garden wall on the northern side of the building	February 2015	Masonry mortar
MG-2	the outer face of the garden wall on the northern side of the building	February 2015	Masonry mortar
MG-3	the lower level of the corner wall of the northern annex (located on the northern façade of the mosque	February 2015	Masonry mortar
MG-4	the lower level of the semi-arched niche located on the façade of the northern annex on the mosque's northern side	February 2015	Masonry mortar
MG-6	at the lower level of the niche located to the right of the main entrance door on the mosque's entrance façade (the west side of the mosque)	February 2015	Masonry mortar
MG-7	the upper level of the oval minaret base inside the tomb structure located on the southern façade of the mosque	February 2015	Masonry mortar
MG-8	the upper level of the wall to the right of the minaret base on the southern façade of the mosque	February 2015	Masonry mortar
MG-9	the interior wall surface of the entrance façade of the mosque's portico (outer narthex) on the west side of the mosque	February 2015	Masonry mortar
MG-10	lower level of the exterior façade at the southeastern corner of the mosque	February 2015	Masonry mortar
MG-12	exterior face of the qibla wall (eastern façade, apse) of the mosque	February 2015	Masonry mortar
MG-13	between the brick and stone elements on the northern exterior façade of the mosque	February 2015	Masonry mortar

Figure 3. Sampling locations of the mortar samples. (**A**) Outer face of the northern garden wall (MG-1 and MG-2). (**B**) Lower level of the corner wall of the northern annex (MG-3). (**C**) Lower level of the semi-arched niche on the northern annex façade (MG-4). (**D**) Lower level of the niche to the right of the main entrance door on the entrance façade (MG-6). (**E**) Upper level of the oval minaret base inside the tomb structure on the southern façade (MG-7). (**F**) Upper level of the wall to the right of the minaret base on the southern façade (MG-8). (**G**) Interior wall surface of the entrance portico on the west side (MG-9). (**H**) Lower level of the exterior façade at the southeastern corner (MG-10). (**I**) Exterior face of the qibla wall (eastern façade, apse) (MG-12). (**J**) Between the brick and stone elements on the northern exterior façade (MG-13).

Analytical Techniques

X-ray diffraction (XRD) analysis was conducted to determine the mineralogical composition of the mortar samples collected from the structure. The composition comprised crushed brick, aggregate, gypsum, and silicate phases present in the bedding mortar. This technique provided valuable insights into the crystalline phases associated with the materials used in the mortar application. To ensure homogeneity, the samples were finely ground and placed in a low-background sample holder to minimize interference. XRD patterns were recorded at room temperature using a Malvern PANalytical Empyrean Series 3 X-ray diffractometer at the Aluminum Testing, Training, and Research Center of Fatih Sultan Mehmet Vakıf University. The instrument was operated with a goniometer speed of 1°/min (2θ) and employed CuKα radiation (λ = 1.5418 Å, 45 kV, 40 mA). Data collection was carried out over a 2θ scan range of 5° to 90°, with a step size of 0.02°, a divergence slit of 0.5 mm, and a receiving slit of 0.3 mm. Phase identification and analysis of the XRD patterns were performed using the Philips X'Pert HighScore Plus software (version 3.0) package (PDF-2 Release 2003) in conjunction with the JCPDS (Joint Committee on Powder Diffraction Standards) database.

FTIR analysis was also performed on the same samples, which had already been finely ground prior to the XRD measurements. Given its capability to identify both organic and inorganic components, including pigments and binders, FTIR is among the most effective techniques for characterizing mortar compositions. To ensure optimal interaction with the ATR crystal, the samples were further ground before analysis. Approximately 5 mg of each sample was used for the measurements. IR spectra were obtained in ATR mode using a Bruker Alpha II spectrometer equipped with a single-bounce diamond ATR accessory and operated with Opus software (version 8.1) at the Research Center for the Conservation of Cultural Property, Fatih Sultan Mehmet Vakıf University. To enhance the signal-to-noise ratio, each spectrum was acquired with 96 scans per sample at a spectral resolution of 4 cm^{-1}. The air spectrum was used as a background reference during measurements. The spectral range spanned from 4000 cm^{-1} to 400 cm^{-1}, covering the mid-infrared region necessary for identifying key functional groups. Background correction was performed prior to each measurement, and the resulting spectra were processed using specialized software for baseline correction and peak identification. This analysis aimed to determine the principal components of the mortars, verify their composition as compared with XRD findings, and assess the extent of carbonation through functional group identification.

3. Results

X-ray diffraction (XRD) analysis of the historic laying mortar identified the presence of calcite ($CaCO_3$), gypsum ($CaSO_4 \cdot 2H_2O$), quartz (SiO_2), albite ($NaAlSi_3O_8$), microcline ($KAlSi_3O_8$), and illite [$(K,H_3O)(Al,Mg,Fe)_2(Si,Al)_4O_{10}(OH)_2$] minerals (Figure 4). Calcite, the primary binding component of historic mortars, forms through the carbonation of lime-based materials. Its most dominant peaks were observed at 2θ values of 29.4° (d ≈ 3.03 Å), 39.5° (d ≈ 2.28 Å), and 43.2° (d ≈ 2.10 Å), which are recognized in the literature (PDF2-Refcode: 01-081-2027) as characteristic peaks of calcite. The presence of gypsum indicated sulfate content in the mortar, with its most prominent peaks detected at 11.5° (d ≈ 7.61 Å), 20.8° (d ≈ 4.29 Å), and 29° (d ≈ 3.07 Å). Quartz, present as an aggregate component in the mortar, exhibited its strongest diffraction peaks at 26.7° (d ≈ 3.34 Å), 20.7° (d ≈ 4.27 Å), and 50.2° (d ≈ 1.82 Å), supporting the presence of natural siliceous compounds (PDF2-Refcode: 00-021-0816). Additionally, albite and microcline, belonging to the feldspar group, were identified in the mortar. The dominant diffraction peaks for albite (PDF2-Refcode: 01-076-0927) were observed at 27.9° (d ≈ 3.19 Å), 22.3° (d ≈ 4.00 Å), and 16.1° (d ≈ 5.47 Å), while those for microcline (PDF2-Refcode: 00-019-0932) were recorded at 27.6° (d ≈ 3.24 Å),

18.2° (d ≈ 4.87 Å), and 40.4° (d ≈ 2.23 Å). Furthermore, illite, an indicator of clay content, was detected, with its strongest diffraction peaks appearing at 8.8° (d ≈ 10.0 Å), 19.7° (d ≈ 4.49 Å), and 26.9° (d ≈ 3.32 Å) (PDF2-Refcode: 00-026-0911). These findings provide valuable insights into the raw materials used in the composition of the historic masonry mortar and reveal its mineralogical characteristics. The XRD analysis results, representing the overall mineralogical composition of the mortar, including both binder and aggregates, indicated the presence of various components and provided critical information about the samples' structural and environmental interactions.

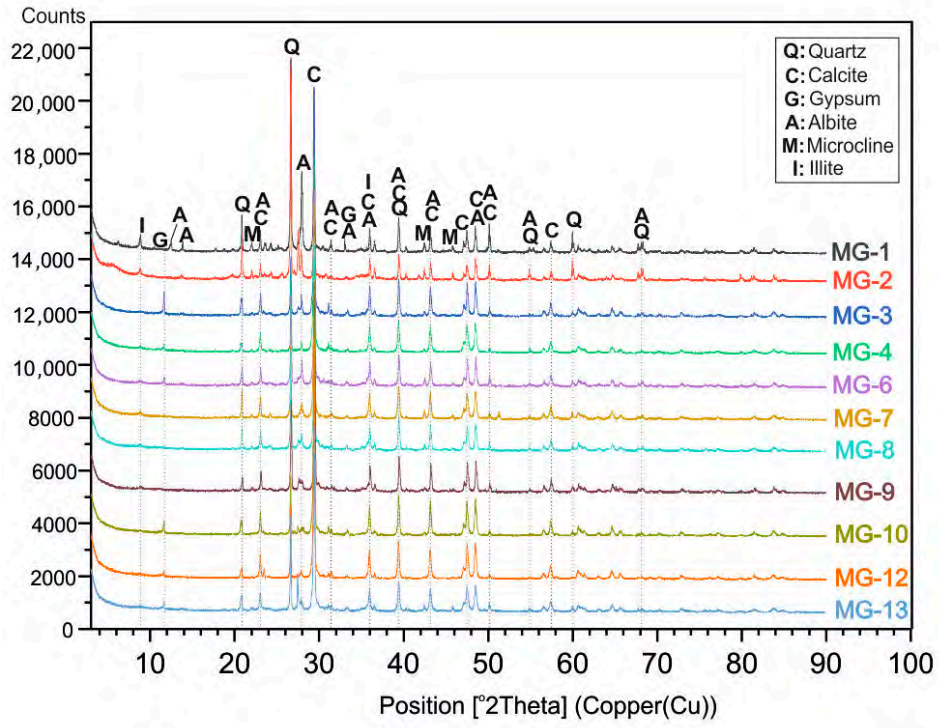

Figure 4. X-ray diffraction pattern of the bulk mortar samples. Identified minerals: calcite (C), gypsum (G), quartz (Q), albite (A), microcline (M), illite (I).

ATR-FTIR analysis of the historic masonry mortar identified dominant absorption bands corresponding to calcite ($CaCO_3$), gypsum ($CaSO_4 \cdot 2H_2O$), and silicate groups (Figure 5). The presence of calcite was confirmed by the characteristic C–O stretching vibration bands of carbonate compounds, observed in the 1400–1460 cm^{-1} range (asymmetric stretching, ν_3), at 875 cm^{-1} (out-of-plane bending, ν_2), and at 712 cm^{-1} (in-plane bending, ν_4) (Figure 5c). The presence of gypsum was determined by the characteristic S–O stretching bands of sulfate groups, detected in the 1000–1100 cm^{-1} region (asymmetric stretching, ν_3) (Figure 5c). Silicate groups, particularly those associated with feldspar and quartz minerals, were identified by broad Si–O–Si stretching vibration bands, observed in the 900–1100 cm^{-1} range (Si–O stretching, ν_3) and the 450–500 cm^{-1} range (Si–O bending, ν_4) (Figure 5c). Additionally, low-intensity carbon dioxide (CO_2) absorption bands were detected in the 2300–2400 cm^{-1} range. Furthermore, broad O–H stretching bands associated with water molecules were observed in the 3200–3500 cm^{-1} region (O–H stretching, ν_3) (Figure 5b). These findings confirm that the ATR-FTIR analysis supports the XRD results and verifies the mineralogical composition of the historic mortar. The distinct spectral features of calcite, gypsum, and silicate components provided valuable insights into the raw materials and binding properties of the mortar.

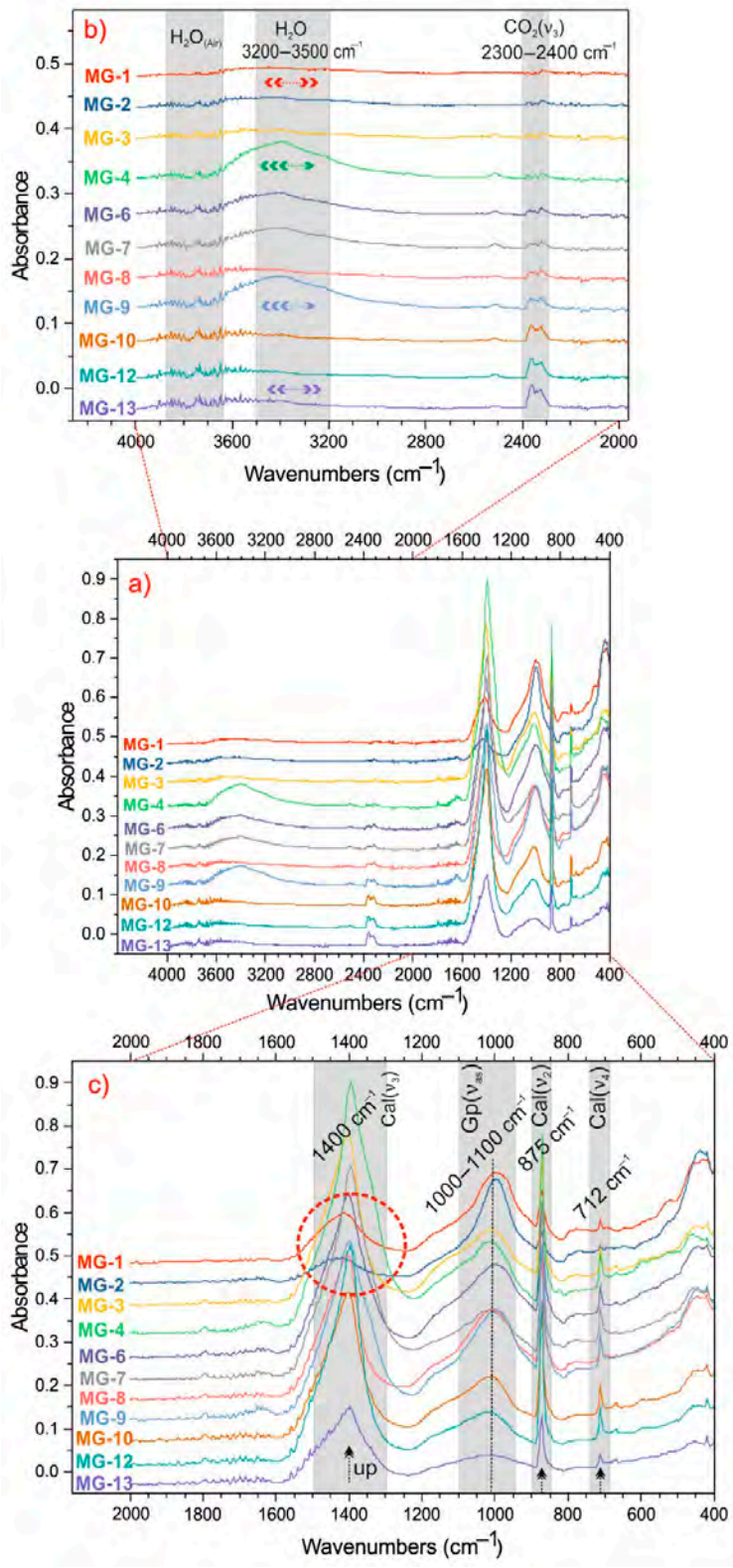

Figure 5. FTIR spectra collected from mortar samples. (**a**) Spectra obtained in the 400–4000 cm^{-1} range. (**b**) Detailed view of the absorption bands in the 2000–4000 cm^{-1} range. (**c**) Detailed view of the dominant absorption bands in the 400–2000 cm^{-1} range. (In (**b**), the broadening in the H_2O band is indicated by arrows in the color corresponding to each spectrum. In (**c**), the shapes of the characteristic peaks attributed to calcite are marked with black arrows as indicators of carbonation degree. Additionally, the incomplete carbonation process of the main calcite peaks in MG-1 and MG-2 samples is highlighted with a red dashed circle in (**c**)).

4. Discussion

The results represent the overall mineralogical composition of the mortar, including both binder and aggregate phases. The distribution and structural characteristics of the minerals identified in the historic masonry mortar samples are of critical importance in understanding the physicochemical behavior and durability of the material. Calcite ($CaCO_3$) was determined as the primary binding component of the mortar. In lime-based mortars, the binding material typically consists of either quicklime (CaO) or slaked lime ($Ca(OH)_2$). Slaked lime gradually reacts with atmospheric carbon dioxide (CO_2), leading to carbonation and the subsequent formation of calcite. This transformation not only facilitates the hardening of the mortar but also enhances the mechanical strength of the structure. The presence of CO_2 absorption bands (2300–2400 cm^{-1}) in ATR-FTIR analysis suggests that the carbonation process remains active and that the mortar has been subjected to atmospheric exposure over time. The detection of gypsum ($CaSO_4 \cdot 2H_2O$) indicates the need to examine the sulfate content of the mortar. Sulfates may originate from the raw materials used during mortar preparation, but they can also be introduced later due to environmental interactions and atmospheric pollution. In particular, calcium compounds present in lime-based mortars can react with atmospheric sulfur dioxide (SO_2), leading to the formation of gypsum. The fact that gypsum was not detected in all samples supports this hypothesis, suggesting that sulfate incorporation is not intrinsic to the original composition of the mortar but rather a consequence of environmental exposure. This phenomenon is particularly prevalent in urban areas with high levels of air pollution, where sulfate-rich deposits accumulate on the surfaces of historic structures. Excessive gypsum formation can lead to expansion and surface deterioration, ultimately compromising the integrity of the material. The sulfate bands observed in ATR-FTIR (1000–1100 cm^{-1}), confirmed by XRD analysis, further support the presence of gypsum in the mortar (Table 2).

In addition to the binding material, aggregate components play a crucial role in enhancing the durability of the mortar. XRD analysis identified quartz (SiO_2), albite ($NaAlSi_3O_8$), and microcline ($KAlSi_3O_8$) as key constituents of the aggregate. The presence of quartz (SiO_2) suggests that the aggregate component was primarily derived from sand or crushed natural stones. Quartz is a hard and chemically stable mineral, which contributes significantly to the long-term durability of mortar. The broad Si–O–Si stretching bands (900–1100 cm^{-1}) observed in ATR-FTIR analysis further support the presence of quartz and silicate compounds in the sample. The presence of feldspar minerals (albite and microcline) indicates that the mortar incorporates rock-derived aggregates. Feldspars could have been introduced into the mortar through weathered rock fragments used as aggregate. Over time, feldspar minerals can undergo alteration due to their alkaline solubility, contributing to the formation of secondary minerals. This mineralogical composition suggests that sand or crushed rock-based aggregates were used in mortar production, enhancing the structural stability of the material.

The detection of illite in the XRD analysis indicated the presence of clay minerals in the mortar. Illite is a secondary clay mineral that can form from the weathering of feldspar minerals and is typically present as a fine-grained component within mortar. The broad O–H stretching bands (3200–3500 cm^{-1}) detected in ATR-FTIR analysis further support the presence of clay minerals, indicating their role in moisture retention within the mortar. The presence of clay minerals enhances the water retention capacity of the mortar, thereby supporting the gradual carbonation process of the lime binder. However, an excessive clay content can alter the shrinkage and expansion properties of the material, potentially increasing the risk of cracking. Therefore, a controlled proportion of clay minerals is essential in historic mortars to ensure both mechanical strength and environmental durability.

Table 2. Summary of minerals and phases identified by XRD and ATR-FTIR analyses.

Mineral/Phase	Technique	Key Features (2θ or ν; cm^{-1})	Interpretation/Function
Calcite ($CaCO_3$)	XRD, ATR-FTIR	2θ: 29.4°, 39.5°, 43.2°; ν: 1400–1460, 875, 712	Main binder formed by carbonation of lime
Gypsum ($CaSO_4 \cdot 2H_2O$)	XRD, ATR-FTIR	2θ: 11.5°, 20.8°, 29°; ν: 1000–1100	Sulfate phase; may indicate environmental interaction
Quartz (SiO_2)	XRD, ATR-FTIR	2θ: 26.7°, 20.7°, 50.2°; ν: 900–1100, 450–500	Silicate aggregate that improves durability
Albite ($NaAlSi_3O_8$)	XRD	2θ: 27.9°, 22.3°, 16.1°	Feldspar aggregate; sodium-rich component
Microcline ($KAlSi_3O_8$)	XRD	2θ: 27.6°, 18.2°, 40.4°	Feldspar aggregate; potassium-rich component
Illite	XRD, ATR-FTIR	2θ: 8.8°, 19.7°, 26.9°; ν: 3200–3500	Clay mineral; enhances moisture retention
Silicates (feldspar and quartz)	ATR-FTIR	ν: 900–1100, 450–500	Supports presence of feldspar and quartz aggregates
CO_2 (absorption)	ATR-FTIR	ν: 2300–2400	Indicates atmospheric CO_2 exposure (carbonation)
Water (O–H bands)	ATR-FTIR	ν: 3200–3500	Related to water content and clay minerals

The observation of sharp and well-defined absorption bands at 712 cm^{-1}, 875 cm^{-1}, and around 1400 cm^{-1} in the FTIR spectra indicated an advanced level of carbonation in the historic laying mortars (marked by red and black arrows in Figure 5c). These bands are characteristic of calcite, with the 1400–1460 cm^{-1} region corresponding to the asymmetric C–O stretching vibration (ν_3), the 875 cm^{-1} band representing out-of-plane bending (ν_2), and the 712 cm^{-1} band associated with in-plane bending (ν_4). The sharp and distinct nature of these bands suggests that the carbonation process has been fully completed over an extended period, resulting in a highly stable mortar matrix. The presence of such well-defined calcite bands confirms that the mortar contains a fully carbonated lime binder, which is an expected characteristic of historic mortars that have been exposed to atmospheric conditions for a long time and gradually stabilized. The qualitative nature of spectral comparison was favored due to the low number of modern samples. However, future studies involving larger datasets will enable robust statistical modeling.

In contrast, the MG-1 and MG-2 samples, taken from the modern extension wall added in the second half of the 20th century (marked by a pink square in Figure 2), exhibited a broader C–O band at around 1400 cm^{-1} (highlighted with a red dashed circle in Figure 5c). This broadening suggests that the carbonation process in these samples is incomplete or proceeding in a less uniform manner. Several factors could contribute to this difference. While historic mortars are typically composed of pure lime ($Ca(OH)_2$) as the binding material, modern extension walls may have used lime mortars with cement additives, which could influence the spectral properties. In cement-containing binders, the C–O absorption band tends to appear broader due to the complex nature of carbonation and the presence of additional mineral phases. However, no cement-related mineral phases or indicators were identified in any of the analyzed samples, suggesting that the MG-1 and MG-2 mortars are lime-based but at an earlier stage of carbonation.

Another possible explanation is the age difference between the mortars. Historic mortars have been exposed to continuous interaction with atmospheric CO_2 for centuries, allowing them to fully carbonate, whereas the relatively younger MG-1 and MG-2 mortars have not yet undergone complete carbonation or fully stabilized their crystal structure. Additionally, carbonation is influenced by environmental factors such as humidity, temper-

ature, and CO_2 concentration. The structural position of the modern extension wall might have limited exposure to air circulation, which could have slowed down the carbonation process. These findings highlight the distinct carbonation states observed in historic versus modern mortars within this study, emphasizing the role of material age and exposure conditions in achieving full carbonation.

The presence of gypsum ($CaSO_4 \cdot 2H_2O$) is also relevant to the discussion of carbonation. The broad and low-intensity bands observed in the 1000–1100 cm^{-1} region suggest that the sulfate content in the mortar is limited and may have accumulated primarily on the surface rather than being an inherent component of the original mix. If sulfates were originally present in significant amounts within the mortar, sharper and more defined gypsum absorption bands would be expected. The formation of gypsum at an early stage of crystallization might also explain why the bands appeared broad rather than well-defined. Additionally, the raw materials used in the production of the mortar may have been low in sulfate content, naturally resulting in a lower gypsum concentration in the final composition.

A further significant observation in the FTIR spectra was the behavior of the O–H stretching bands (3200–3500 cm^{-1}). In most samples, these bands appeared broad and weak (indicated by green and blue arrows in Figure 5b) or were nearly absent (marked by red and purple arrows in Figure 5b). This suggests that the mortar has undergone extensive drying and has a low moisture content. Fully carbonated mortars typically lose most of their bound water over time, which is consistent with these findings. Additionally, a low clay content could further reduce the moisture retention capacity of the mortar. Prolonged exposure to environmental conditions may have resulted in the evaporation of water molecules within the binder matrix, leading to the observed spectral characteristics. However, if a high clay content were present in the samples, more distinct O–H absorption bands would be expected. The fact that strong water-related bands were not observed suggests that the historic mortars have experienced a gradual reduction in water retention capacity, becoming mechanically drier and more structurally stable over time. While further compositional analyses such as TGA or SEM-EDX would clarify binder differences, the current study focused on spectroscopic features, which nonetheless revealed clear transformation gradients. Although pH measurements were not performed in this study, future research is encouraged to correlate spectroscopic findings with pH variations across different time-dependent exposure zones.

The practical significance of this study lies in its direct contribution to material selection and restoration planning in heritage conservation. By revealing differences in carbonation maturity between historical and modern mortars, the findings provide a scientific basis for evaluating the long-term performance and chemical compatibility of repair materials. This is particularly important in restoration contexts where mismatched materials can accelerate deterioration rather than prevent it. The dual application of XRD and ATR-FTIR offers a non-destructive and accessible methodology that can be adopted by conservators and materials scientists to inform decisions regarding mortar formulation, intervention timing, and overall conservation strategy. As such, the methodological approach proposed here not only contributes to academic knowledge but also serves as a practical diagnostic tool in the field. The distinction between carbonation levels in historical and modern mortars allows conservators to predict the long-term behavior of repair mortars and avoid premature failure in restoration projects. The spectroscopic insights presented here can be used as diagnostic benchmarks in future conservation campaigns.

5. Conclusions

These analytical results indicate that the carbonation process in historic mortars has reached an advanced and fully completed stage, whereas carbonation in modern extension wall mortars remains incomplete. The sharpness of the calcite bands in historic mortars confirms full carbonation and the stabilization of the mineral structure. In contrast, the broader C–O band at 1400 cm^{-1} in the MG-1 and MG-2 samples suggests that the carbonation process is still in progress and the crystal lattice of calcite is not yet fully stabilized. The slightly broad gypsum bands indicate that sulfate accumulation is limited and primarily surface-related. Additionally, the weak water absorption peaks suggest that the mortars have significantly dried and aged over time. These findings demonstrate that the carbonation process in the historic mortars has been completed over the long term, whereas the modern extension mortars have not yet fully undergone this transformation.

This study demonstrates the effectiveness of a combined XRD and ATR-FTIR approach in evaluating carbonation maturity and secondary phase formation in historic lime-based mortars. The comparative analysis revealed that modern intervention mortars exhibit a lower degree of carbonation than original mortars, underscoring their limited compatibility. These findings offer a practical and scientifically supported basis for selecting restoration materials that align with the chemical and structural characteristics of historic substrates, contributing to more durable and sustainable conservation practices.

Author Contributions: Conceptualization, İ.C. and E.K.; methodology, İ.C. and E.K.; software, E.K.; validation, E.K., İ.C.; investigation, İ.C. and E.K.; resources, E.K.; data curation, İ.C. and E.K.; writing—original draft preparation, İ.C. and E.K.; writing—review and editing, E.K.; visualization, İ.C.; supervision, İ.C.; project administration, İ.C. All authors have read and agreed to the published version of the manuscript.

Funding: This research did not receive any external funding. Additionally, the APC was funded by the budget of the Research Center for the Conservation of Cultural Property of Fatih Sultan Mehmet Vakıf University.

Data Availability Statement: The data presented in this study are available on request from the corresponding author.

Acknowledgments: As the authors of this article, we would like to express our gratitude to Fatih Özbaş and Mesut İş from the Research Center for the Conservation of Cultural Property, who contributed to the sample collection during this study conducted for the Molla Şemsettin Gürani Mosque Material Analysis and Conservation Report (2015) and who continue to work at the Center.

Conflicts of Interest: The authors declare no conflict of interest.

References

1. Soysal, U.; Altınışık, D.D. Tarihi Kireç Harçları ve Karakterizasyonu Çalışmaları Üzerine İncelemeler. *J. Technol. Appl. Sci.* **2024**, *7*, 97–115. [CrossRef]
2. Kesikidou, F.; Matamadiotou, I.; Stefanidou, M. Influence of Accelerated Carbonation on the Physico-Mechanical Properties of Natural Fiber-Reinforced Lime Mortars. *Materials* **2024**, *17*, 4461. [CrossRef] [PubMed]
3. Boynton, R.S. *Chemistry and Technology of Lime and Limestone*, 2nd ed.; Wiley: New York, NY, USA, 1980. Available online: https://www.wiley.com/en-us/Chemistry+and+Technology+of+Lime+and+Limestone%2C+2nd+Edition-p-9780471027713 (accessed on 2 July 2025).
4. Riccardi, M.P.; Duminuco, P.; Tomasi, C.; Ferloni, P. Thermal, microscopic and X-ray diffraction studies on some ancient mortars. *Thermochim. Acta* **1998**, *321*, 207–214. [CrossRef]
5. Richardson, L., Jr. *A New Topographical Dictionary of Ancient Rome*; Johns Hopkins University Press: Baltimore, MD, USA, 1992. Available online: https://www.press.jhu.edu/books/title/1037/new-topographical-dictionary-ancient-rome (accessed on 2 July 2025).
6. Moropoulou, A.; Bakolas, A.; Anagnostopoulou, S. Composite materials in ancient structures. *Cem. Concr. Compos.* **2005**, *27*, 295–300. [CrossRef]

7. Moropoulou, A.; Bakolas, A.; Bısbıkou, K. Invesatigation of the Technology of Historic Mortars. *J. Cult. Herit.* **2000**, *1*, 45–58. [CrossRef]
8. Stefanidou, M.; Papayianni, I. The role of aggregates on the structure and properties of lime mortars. *Cem. Concr. Compos.* **2005**, *27*, 914–919. [CrossRef]
9. Rodríguez-Navarro, A.B.; Domínguez-Gasca, N.; Muñoz, A.; Ortega-Huertas, M. Change in the chicken eggshell cuticle with hen age and egg freshness. *Poult. Sci.* **2013**, *92*, 3026–3035. [CrossRef] [PubMed]
10. Centeno, S.A.; Shamir, J. Surface enhanced Raman scattering (SERS) and FTIR characterization of the sepia melanin pigment used in works of art. *J. Mol. Struct.* **2008**, *873*, 149–159. [CrossRef]
11. De Benedetto, G.E.; Laviano, R.; Sabbatini, L.; Zambonin, P.G. Infrared spectroscopy in the mineralogical characterization of ancient pottery. *J. Cult. Herit.* **2002**, *3*, 177–186. [CrossRef]
12. Raphael, L. Application of FTIR spectroscopy to agricultural soils analysis. In *Fourier Transforms—New Analytical Approaches and FTIR Strategies*; IntechOpen: London, UK, 2011; pp. 385–404.
13. Satyanarayana, G.V.V.; Dakshina Murthy, N.R. Behavior of Blended Mortars Under Acid Environment. *IUP J. Struct. Eng.* **2013**, *6*.
14. Downs, R.T. The RRUFF Project: An integrated study of the chemistry, crystallography, Raman and infrared spectroscopy of minerals. In Proceedings of the Program and Abstracts of the 19th General Meeting of the International Mineralogical Association, Kobe, Japan, 23–28 July 2006.
15. Elert, K.; Rodríguez-Navarro, C.; Sebastian, E.; Hansen, E.; Cazalla, O. Lime mortars for the conservation of historic buildings. *Stud. Conserv.* **2002**, *47*, 62–75. [CrossRef]
16. do Rosário Veiga, M.; Fragata, A.; Velosa, A.L.; Magalhães, A.C.; Margalha, G. Lime-based mortars: Viability for use as substitution renders in historical buildings. *Int. J. Archit. Herit.* **2010**, *4*, 177–195. [CrossRef]
17. Jordán, M.M.; Jordá, J.; Pardo, F.; Montero, M.A. Mineralogical analysis of historical mortars by FTIR. *Materials* **2018**, *12*, 55. [CrossRef] [PubMed]
18. Al Sekhaneh, W.; Shiyyab, A.; Arinat, M.; Gharaibeh, N. Use of FTIR and thermogravimetric analysis of ancient mortar from The Church of the Cross in Gerasa (Jordan) for conservation purposes. *Mediterr. Archaeol. Archaeom.* **2020**, *20*, 159.
19. Muller-Wiener, W. *Istanbul'un Tarihsel Topografyasi: 17. Yuzyil Baslarina Kadar Byzantion-Konstantinopolis-Istanbul*; Yapi Kredi Yayinlari: Istanbul, Turkey, 2007.
20. Esmer, M. İstanbul'daki Orta Bizans Dönemi Kiliseleri ve Çevrelerinin Korunması İçin Öneriler. Ph.D. Thesis, Istanbul Technical University, Istanbul, Türkiye, 2012. Volume 596.
21. Hallensleben, Z. Annexbauten der Kilise camii in Istanbul. *MDAI(I)* **1965**, *XV*, 323–330.
22. Available online: https://tr.wikipedia.org/wiki/Vefa_Kilise_Camii#/map/0 (accessed on 2 July 2025).
23. Available online: https://www.thebyzantinelegacy.com/vefa (accessed on 2 July 2025).
24. Efendi, A.H.; Efendi, A.S.; Efendi, S.B. *İstanbul Camileri ve Diğer Dini Sivil Mimari Yapıları Hadikatü'l Cevami, haz. AN Galitekin*; İşaret Yayınları: İstanbul, Turkey, 2001.
25. Nomidis, M.I. Rapport Preliminaire des Travaux Executes dans une Eglise Byzantine (Kilise Camii). *Notre Dame D'ephese* **1958**, *2*, 14–19.
26. Fatih Sultan Mehmet Vakıf University—Research Center for the Conservation of Cultural Property. *Molla Şemsettin Gürani Mosque Material Analysis and Conservation Report*; Fatih Sultan Mehmet Vakıf University—Research Center for the Conservation of Cultural Property: Istanbul, Türkiye, 2015; *unpublished*. (In Turkish)